An Analytical Small-Signal Bias-Dependent Nonuniform Model for p-i-n Traveling-Wave Photodetectors

Guido Torrese, *Associate Member, IEEE*, Isabelle Huynen, *Member, IEEE*, Marc Serres, Dominic Gallagher, Matthew Banham, and André Vander Vorst, *Life Fellow, IEEE*

***Abstract*—A fully analytical small-signal model is developed for the frequency response of traveling-wave photodetectors. It takes into account the dependence of the equivalent transmission-line admittance on the position, induced by the nonuniform distribution of the optical beam along the traveling direction. Moreover, the influence of the bias voltage on the transit time has been accurately investigated. The model is applied to the design of an InAlAs–InGaAs p-i-n photodetector. Its performances are investigated in term of electrical bandwidth.**

***Index Terms*—Bandwidth, saturation regime, traveling-wave photodetector (TWPD).**

I. Introduction

OVER THE LAST years, interest for high-speed traveling-wave photodetectors (TWPDs) has increased [1]–[3]. These devices are expected to play an important role in the optical communication field because, unlike vertically illuminated p-i-n photodiodes (VPDs), they can achieve a large bandwidth-efficiency product. As a matter of fact, to increase the VPD bandwidth, the carrier transit time must be minimized, while a thick intrinsic region is necessary for light absorption [4]. Moreover, traditional p-i-n photodiodes are limited by an *RC* time constant. The general outline of TWPDs consists of an electrical coplanar transmission line coupled to an optical waveguide. The electrical field is applied perpendicular to the photon path, hence, bandwidth and internal quantum efficiency can be optimized separately. If matching condition between the optical and electrical signal traveling along the photodetector is achieved, the usual *RC* time constant cannot be defined and the main limit on the bandwidth is due to reflections at the input and output ends of the structure. As discussed in [2], propagation on TWPDs is quasi-TEM. Transmission-line equivalent circuits describing the properties of quasi-TEM waveguides have been extensively investigated in the literature [2], [3]. It should, however, be noted that both the impedance and shunt admittance of these proposed equivalent circuits not only are independent of the light source characteristics, but also of the external reverse voltage used to bias the photodetector. Another important feature of p-i-n devices is that the junction transit time generally depends on the reverse voltage. Although the basic theory on traveling-wave solid-state device has been previously published by Soohoo *et al.* [5], it applies to a simple case when detectors operate at an electric field large enough to saturate the carrier velocity. The same hypothesis has been utilized by Huynen *et al.* [6] and Huynen and Vander Vorst [7]. Moreover, results provided in [7] have been obtained by neglecting the influence of the transit time.

The small-signal model presented in this paper takes into account the nonuniformity of the shunt-distributed admittance of the line induced by the exponential decrease of light power along the optical traveling path, and the influence on the transit time of the bias voltage, enabling the prediction of the TWPD behavior in both a saturated and unsaturated regime. In Section II, we present in detail the distributed equations for investigating the behavior of TWPDs. We formally derive an expression for the current density and we obtain an RF transmission-line model depending on the loads at the input and output ends of the device. In Section III, we optimize the TWPD geometry for optical conversion. Section IV illustrates the efficiency of the model by comparison with simulations using previously published models.

Manuscript received July 12, 2001; revised December 21, 2001. This work was supported by the Belgian Federal Office for Scientific, Technical, and Cultural Affairs under the PAI-IV/13 Project. This work was supported in part by the National Fund for Scientific Research, Belgium, and by the Ministry of Education of the Grand Duchy of Luxembourg.

G. Torrese, I. Huynen, and A. Vander Vorst are with the Microwave Laboratory, Université Catholique de Louvain, B-1348 Louvain-la-Neuve, Belgium (e-mail: huynen@emic.ucl.ac.be).

M. Serres was with the Microwave Laboratory, Université Catholique de Louvain, B-1348 Louvain-la-Neuve, Belgium. He is now with HITEC Luxembourg S.A., L-1458 Luxemburg, Grand-Duchy of Luxemburg (e-mail: marc.sarres@hitec.lu).

D. Gallagher is with Photon Design, OX4 1TW Oxford, U.K. (e-mail: dfgg@photond.com).

M. Banham was with Photon Design, OX4 1TW Oxford, U.K. He is now with Blaze Photonics, BA2 7AY Bath, U.K.

Digital Object Identifier 10.1109/TMTT.2002.804640

II. TWPD Model

A. Determination of the Small-Signal Current

In order to investigate the behavior of TWPDs, we divide the photodetector into differential sections of length Δz and we then determine for each section the total current density as the sum of drift and displacement components. Essentially, the total current density is calculated from a one-dimensional model in the x-direction. The whole device is obtained by repeating n times a section in the z-direction, as with traditional transmission lines. If a section is sufficiently short, we can consider that

the absorbed light is constant. Assuming no back-reflection at the end of structure, the optical generation rate is

$$G(z,t) = G_0 + G_a\left(e^{-(\alpha_o + j\beta_o)z + j\omega t}\right) \tag{1}$$

where the optical absorption coefficient α_o and propagation coefficient β_o are defined according to [6]. In (1), ω is the RF angular frequency, while G_0 and G_a represent the signal amplitude of the dc and ac components, respectively. As we consider a side illumination with uniform distribution in the $x-y$-plane, the generation term $G(z,t)$ is x- and y-independent.

In order to determine the total current density, a perturbational approach [8] has been used to solve the transport equations. We assume that all variables can be written as the sum of a dc or time-average part and an ac or time-dependent part. Further, in agreement with the small-signal analysis, it is assumed that the ac quantities are very small in comparison with the dc ones. These hypotheses allow us to decouple the transport equations into zeroth- and first-order equations, then the dc or nonperturbational equations are solved first. As shown in [9], when considering a constant electric field versus the $x-y$ section of the intrinsic region, and when neglecting the carrier recombination, the total current density can be determined in an analytical fashion. To derive the analytical closed form for the current density, we also neglected the charge trapping mechanism, although it should be taken into account for accurate modeling. The dc and ac current densities are, respectively,

$$J_0(x,z) = qE_0\left(n_0\mu_{n0} + p_0\mu_{p0}\right) \tag{2}$$

and

$$\begin{aligned} J_a(x,z) = j\omega\epsilon_s E_a + q\big(&E_a(n_0\mu_{n0} + p_0\mu_{p0}) \\ &+ E_0(n_a\mu_{n0} + n_0\mu_{na} + p_a\mu_{p0} \\ &+ p_0\mu_{pa})\big) \end{aligned} \tag{3}$$

where n and p represent the electron and hole carrier densities, respectively, μ_n and μ_p represent the electron and hole mobilities, E represents the electric field, q represents the electron charge, and ε_s represents the material permittivity, while the subscripts 0 and a indicate the unperturbated (dc) and perturbated (ac) variables, respectively. Equations (2) and (3) are very similar to those in [9], with the exception made that carrier densities and electric fields are now z-dependent because of the optical generation rate (1). In (2) and (3), the transit time is taken into account since carrier mobilities appear. Also, the used mobility model depends on the electric field. Consequently, our model allows us to simulate p-i-n devices outside the saturation regime. Now, integrating (3) with respect to the x variable between 0 and d, and multiplying by (w/d), the ac current can be rewritten as

$$I_a = \frac{w}{d}\int_0^d J_a(x,z)dx = -Y_a V_a + \left(\frac{w}{d}\right)Be^{-z(\alpha_o + j\beta_o)} \tag{4}$$

where d is the thickness of the intrinsic region and w is the width of the photodetector, while the admittance per-unit-length $Y_a\ (S/m)$ is given by

$$Y_a = \left(\frac{w}{d}\right)\left(Ae^{-\alpha_o z} + j\omega\epsilon_s\right) \tag{5}$$

while the A and B terms result in the following:

$$A = \frac{q\alpha_o\,\eta_i P_o}{2Sh\nu E_0\mu_{n0}\omega^2\mu_{p0}}\left(A_1 + A_2 + \frac{2(A_3 + A_4)}{d}\right) \tag{6}$$

$$B = -\frac{E_0 q\alpha_o\,\eta_i P_a}{Sh\nu\omega^2}B_1 \tag{7}$$

with coefficients $A_1 - A_4$ and B_1 given in the Appendix. In (6) and (7), P is the incident optical power, S is the illuminated surface, η_i is the internal quantum efficiency, h is the Planck's constant, and ν is the optical frequency. The term B represents the distributed current source due to the photogeneration process. It should be noted that when no light is applied, both A and B are zero, so that the ac current is only due to the displacement mechanism.

B. Nonuniform Transmission-Line Model

As shown in [2], waves propagating along a TWPD are characterized by electric and magnetic field that are quasi-transverse. As only the x-component of the ac electric field is taken into account for each section, we can assume that $E_y = E_z \approx 0$ and that no variation of the E_x component occurs in the y-direction. Hence, by noting that the current flows only in the x-direction, the time–harmonic form of the two curl Maxwell's equations can be combined into

$$\frac{\partial E_x^2}{\partial^2 z} - j\omega\mu_s J_a(x,z) = 0. \tag{8}$$

Thus, the TWPD behavior can be completely determined once that we know the current density $J_a(x,z)$. Integrating (8) in the x-direction and using (4) yields a second-order linear nonhomogeneous differential equation, which is solved for the small-signal voltage $V_a(z)$ as a function of an optical power dependent source term

$$\frac{\partial V_a^2}{\partial^2 z} - \gamma_{\rm rf}^2 V_a = -Z_a B\frac{w}{d}e^{-(\alpha_o + j\beta_o)z} \tag{9}$$

where the complex propagation coefficient $\gamma_{\rm rf}$ and characteristic impedance Z_c are

$$\gamma_{\rm rf}(z) = \sqrt{Z_a Y_a(z)} \text{ and } Z_c(z) = \sqrt{\frac{Z_a}{Y_a(z)}} \tag{10}$$

with an impedance per-unit-length (Ω/m)

$$Z_a = \frac{j\omega\mu_s d}{w}. \tag{11}$$

As show by (5), the admittance per-unit-length Y_a is position dependent, unless no light is applied. On the other hand, the impedance per-unit-length Z_a can be assumed position independent as the light effect does not largely affect its value. It can be determined as suggested in [2], although a full-wave analysis

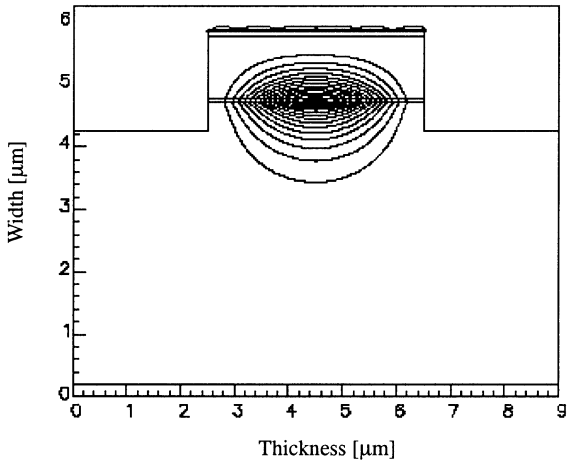

Fig. 1. Two-dimensional view of the traveling-wave topology analyzed using Fimmwave software. The lines show the contour of the equal optical intensity. Geometrical parameters are: thickness of intrinsic area $d = 0.87$ μm, width of mesa structure $w = 4$ μm, section $S = wd$. Optical refraction index computed by Fimmwave is $n_{\text{eff}} = 3.512$.

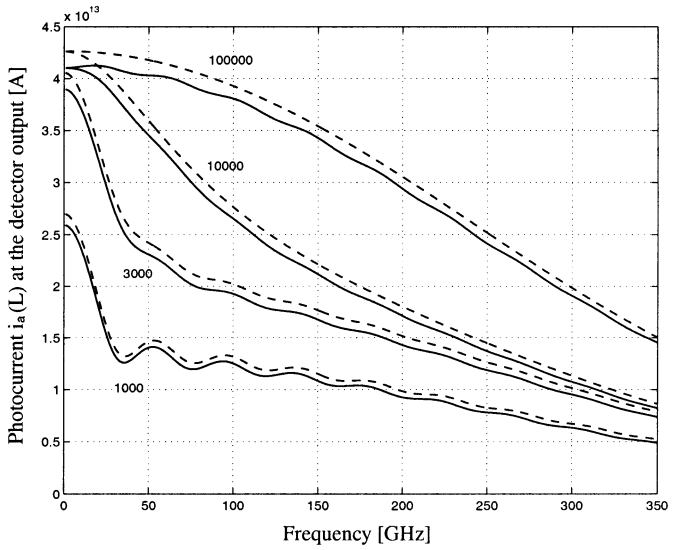

Fig. 2. Output current of input open-ended TWPD ($Y_o = 0$, $Y_L = 1/Z_c = 1/(7.18\ \Omega)$) for four different values of optical absorption coefficient. Geometrical parameters are: $d = 0.2$ μm, $w = 3$ μm, length $L = 1$ mm. Electrical and optical parameters are $n_{\text{opt}} = n_{\text{rf}} = 3.5$, optical wavelength $\lambda_{\text{opt}} = 1.06$ μm, ac modulation of optical power $P_{\text{ac}} = 0.001$ nW, bias voltage $V = 10$ V. Solid lines are for the present model, while dashed lines correspond to the model presented in [6].

is required for rigorous modeling [10]. The solution of the differential (9) has been determined analytically by the method of variation of parameters, although a more elegant solution can be found by using the Green's function technique, as done by Soohoo *et al.* in [5]. However, in comparison with results provided in [5], the solution of (9) is more complex because of nonuniformity of the transmission line. Finally, the solution of (9) depends on two unknowns constants, which are fixed by applying the following conditions at the two ends of the TWPD:

$$\frac{I_a(0)}{V_a(0)} = Y_o \text{ and } \frac{I_a(L)}{V_a(L)} = -Y_L \tag{12}$$

where Y_o and Y_L are the admittance of the ending loads at the input and output of the device, respectively.

III. Optical Design

The model presented in Section II can be used for device optimization. Fig. 1 shows the intensity field profile of the fundamental TE optical mode obtained by using the software Fimmwave from Photon Design, Oxford, U.K., together with the cross section of the TWPD optimized for 1.33-μm operation. The intrinsic region has been designed by sandwiching a high refractive $In_{0.53}$–$Ga_{0.47}As$ region between two $In_{0.52}Al_{0.48}As$ layers. By adjusting the active layer thickness, the confinement factor is tailored to concentrate the field inside the intrinsic region, while a single quantum well with a large absorption coefficient allows to absorb the optical radiation in a few micrometers. The Fimmwave simulation yields an effective modal index of 3.512 in the intrinsic region by using a rigorous fully vectorial solution of Maxwell's equations.

IV. Results

Fig. 2 shows the output current frequency response for four different values of the optical absorption coefficient α_o: 10^3, 3×10^3, 10^4, and 10^5 m^{-1}. The photodetector has been left open at the input end ($Y_o = 0$) and the output end has been matched to the characteristic impedance ($Y_L = Y_c$). Curves have been traced by using two different models: solid lines show the results obtained with the present model, while dashed lines represent a combination of previously published models [6], [7]. They use simplified equations for the carrier motion within the intrinsic region [6]. Despite the fact that the dashed model assumes no z-dependence of the distributed characteristic impedance and propagation constant and is valid in saturation regime only, an excellent agreement is observed between the two models. This is because the bias voltage V taken equal to 10 V is sufficient to saturate the μ_n and μ_p carrier mobilities. Moreover, we used an extremely low optical power P_a in order to avoid nonlinear saturation effects. Consequently, the z-dependent term in (5) is 13 orders of magnitude less than the uniform term. Under these assumptions, the small discrepancies between solid and dashed lines have to be attributed to the different models used for the carrier motion in the p-i-n junction. Fig. 2 also shows that for values of α_o equal or greater than 10^4 m^{-1}, the light absorption is total since the photogenerated current for those values converge at low frequencies. The bandwidth is maximal for the highest value of α_o because the distributed photogenerated current concentrates at the input of the TWPD. Thus, the bandwidth limitation due to phase mismatch between forward distributed photogenerated current waves and reverse ones generated at the open end is reduced [7]. Hence, for $\alpha_o = 10^5$ m^{-1}, the device response is only limited by the carrier transit time.

Fig. 3 illustrates the influence on the bandwidth of the thickness d of the intrinsic area, and of the mismatch between the output load and characteristic impedance. It first compares the matched output-end frequency response for $d = 0.2$ μm (- · - ·) and $d = 1.0$ μm (- - -): the characteristic impedance depends on d; hence, the output load Z_L is taken different for the two simulated curves to ensure matching. The model verifies that

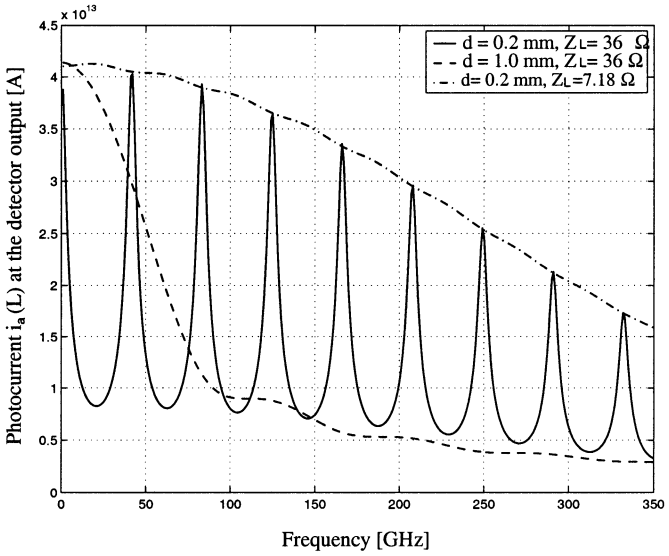

Fig. 3. Output current of input open-ended TWPD for three different combinations of intrinsic thickness d and output load Z_L: ($d = 0.2$ μm, $Z_c = Z_L = 7.18$ Ω): curve (- · - ·), ($d = 1.0$ μm, $Z_L = Z_c = 36$ Ω): curve (- - - -), ($d = 0.2$ μm, $Z_c = 7.18$ Ω, $Z_L = 36$ Ω): curve (—). Geometrical parameters are: $w = 3$ μm, $L = 1$ mm. Electrical and optical parameters are $n_{\rm opt} = n_{\rm rf} = 3.5$, $\lambda_{\rm opt} = 1.06$ μm, $\alpha_o = 2 \times 10^6$ m^{-1}, $P_{\rm ac} = 0.001$ nW, $V = 10$ V.

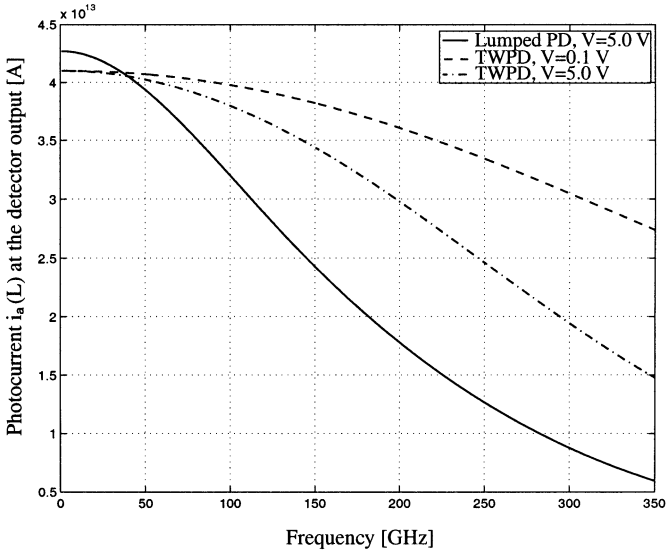

Fig. 4. Comparison between input open-ended TWPD ($Y_o = 0$, $Y_L = 1/Z_c = (1/7.18)S$) for two different values of bias voltage $V = 0.1$ V (- - -), 5 V (- · - ·), and side-illuminated lumped PD with $V = 5$ V (—). Geometrical parameters are: $d = 0.2$ μm, $w = 3$ μm, $L = 0.1$ mm. Electrical and optical parameters are $n_{\rm opt} = n_{\rm rf} = 3.5$, $\lambda_{\rm opt} = 1.06$ μm, $\alpha_o = 10^5$ m^{-1}, $P_{\rm ac} = 0.001$ nW.

increasing the thickness of the intrinsic region reduces the bandwidth because the carrier transit time increases. Solid lines show the current response obtained for $d = 0.2$ μm, but with the output load impedance Z_L equal to the characteristic impedance for a 1-μm-thick intrinsic region. Due to mismatch, a strong ripple occurs in the frequency response.

Fig. 4 illustrates the influence on the bandwidth of the biasing voltage V. First, varying the voltage from 5 V (curve - · - ·) down to 0.1 V (curve - - -) increases the bandwidth. This shows the sensitivity of the model to the bias conditions of the p-i-n junction. Finally, the solid curve (—) shows the frequency response of lumped photodetector of same cross section, illuminated in a similar way: in this case, the junction capacitance effect predominates, which reduces the bandwidth, compared to the TWPD operation mode (- · - ·).

V. Conclusions

This paper has presented a fully analytical nonuniform model for analyzing the bandwidth of p-i-n TWPDs. The model shows first that the nonuniformity in the distributed admittance has no significant influence. Also, it enables to optimize the bandwidth and quantum efficiency of the device by adjusting the absorption coefficient, geometry of the intrinsic region, output load impedance, and bias voltage.

Appendix

$$A_1 = \left((-\beta_p E_0 - 2\,\mu_{p0})\,\mu_{n0} - \beta_n E_0 \mu_{p0} \right) \omega^2 d \tag{13}$$

$$A_2 = 2j\mu_{p0}\mu_{n0}\omega E_0 \left((\beta_p + \beta_n) E_0 + \left(\mu_{n0} + \mu_{p0} \right) \right) \tag{14}$$

$$A_3 = \left(-e^{j\omega d / E_0 \mu_{n0}} + 1 \right) \mu_{p0} {E_0}^2 {\mu_{n0}}^2 \left(\mu_{n0} + E_0 \beta_n \right) \tag{15}$$

$$A_4 = \left(1 - e^{j\omega d / E_0 \mu_{p0}} \right) \mu_{n0} {\mu_{p0}}^2 {E_0}^2 \left(\beta_p E_0 + \mu_{p0} \right) \tag{16}$$

$$B_1 = \left(\left(1 - e^{j\omega d / E_0 \mu_{p0}} \right) {\mu_{p0}}^2 + \left(1 - e^{j\omega d / E_0 \mu_{n0}} \right) {\mu_{n0}}^2 \right) E_0 + j\omega d (\mu_{n0} + \mu_{p0}) \tag{17}$$

and

$$\beta_{n,p} = \left. \frac{d\mu_{n,p}}{dE} \right|_{E = E_0}. \tag{18}$$

References

[1] K. Giboney, R. Nagarajan, T. Reynolds, S. Allen, R. Mirin, and M. Rodwell, "Traveling-wave photodetectors with 172-GHz bandwidth-efficiency product," *IEEE Photon. Technol. Lett.*, vol. 7, pp. 412–414, Apr. 1995.

[2] K. S. Giboney, M. J. W. Rodwell, and J. E. Bowers, "Traveling-wave photodetectors theory," *IEEE Trans. Microwave Theory Tech.*, vol. 45, pp. 1310–1319, Aug. 1997.

[3] V. M. Hietala, G. A. Vawter, T. M. Brennan, and B. E. Hammons, "Traveling-wave photodetectors for high-power large-bandwidth applications," *IEEE Trans. Microwave Theory Tech.*, vol. 43, pp. 2291–2298, Sept. 1995.

[4] J. E. Bowers and C. A. Burrus, Jr., "Ultrawide-band long wavelength p-i-n photodetectors," *J. Lightwave Technol.*, vol. LT-5, pp. 1339–1350, Oct. 1987.

[5] J. Soohoo, S.-K. Yao, J. E. Miller, R. R. Shurtz, II, Y. Taur, and R. A. Gudmundsen, "A laser-induced traveling-wave device for generating millimeter waves," *IEEE Trans. Microwave Theory Tech.*, vol. MTT-29, pp. 1174–1182, Nov. 1981.

[6] I. Huynen, A. Salamone, and M. Serres, "A traveling-wave model for optimizing the bandwidth of p-i-n photodetectors in silicon-on-insulator technology," *IEEE J. Select. Topics Quantum Electron.*, vol. 4, pp. 953–963, Nov.–Dec. 1998.

[7] I. Huynen and A. Vander Vorst, "A four-port scattering matrix formalism for p-i-n traveling wave photodetectors," *IEEE Trans. Microwave Theory Tech.*, vol. 48, pp. 1007–1016, June 2000.

[8] S. E. Laux, "Techniques for small-signal analysis of semiconductor devices," *IEEE Trans. Electron Devices*, vol. ED-32, pp. 2028–2037, Oct. 1985.

[9] G. Torrese, A. Salamone, I. Huynen, and A. Vander Vorst, "A fully analytical model to describe the high-frequency behavior of p-i-n photodiodes," *Microwave Opt. Technol. Lett.*, vol. 31, pp. 329–333, Dec. 2001.
[10] T. Shibata and E. Sano, "Characterization of MIS structure coplanar transmission lines for investigation of signal propagation in integrated circuits," *IEEE Trans. Microwave Theory Tech.*, vol. 38, pp. 881–890, July 1990.

Guido Torrese (S'00–A'01) was born in Genova, Italy, on September 21, 1971. He received the Electronic Engineering degree from the Università degli Studi di Genova, Genova, Italy, in 1997, and the Ph.D. degree in applied sciences from the Université Catholique de Louvain (UCL), Louvain-la-Neuve, Belgium, in 2002.

Since 1997 he has been with the Microwave Laboratory (EMIC), UCL. His research interests include simulation, design, and modeling of p-i-n photodetectors in gallium–arsenide technology. His research also concerns the performance optimization of high-speed optoelectronic detectors and their reliability.

Isabelle Huynen (S'90-A'95–M'96) was born in Brussels, Belgium, in 1965. She received the Electrical Engineer degree and Ph.D. degree in applied sciences from the Université Catholique de Louvain (UCL), Louvain-la-Neuve, Belgium, in 1989 and 1994, respectively.

In 1989, she joined the Microwave Laboratory, UCL, where she is currently a Research Associate of the National Fund for Scientific Research (FNRS), Belgium, and a Part-Time Associate Professor. Her main research deals with electromagnetic theory and measurement techniques applied to materials, devices, and circuits at microwave, millimeter-wave, and optical wavelengths. She has particular interest in the development of microwave and millimeter-wave devices based on nanoscaled materials and topologies, in view of synthesizing wide-band hybrid and integrated opto-electronic circuits for telecommunications applications.

Dr. Huynen is a member of the Belgian Society of Telecommunication and Electronic Engineers (SITEL) and the Royal Society of Belgian Electricians (SRBE/KVBE).

Marc Serres was born in Erlangen, Germany, in 1972. He received the Electrical Engineer degree and Ph.D. degree in applied sciences from the Université Catholique de Louvain (UCL), Louvain-la-Neuve, Belgium, in 1995 and 1999, respectively.

His research interests included modeling and characterization of ultra-wide-band opto-electrical and electrooptical transducers in the field of optical control of microwave devices and optical communication systems. He is currently involved in large antenna design for satellite communications at HITEC Luxembourg S.A., Luxemburg, Grand-Duchy of Luxemburg.

Dominic Gallagher was born in Swansea, U.K., in 1962. He received the B.A. and Ph.D. degrees from the University of Cambridge, Cambridge, U.K., in 1984 and 1987, respectively.

He then became a Research Fellow involved with optical logical elements in laser diode-based devices. He then spent two years with the Fraunhofer Institute for Applied Solid-State Physics (IAF), Freiburg, Germany, where he was involved with laser diodes and grating devices. In 1992, he founded Photon Design, Oxford, U.K.

Matthew Banham received the M.Sci. degree in physics and astronomy from The University of Nottingham, Nottingham, U.K., in 1999.

He spent three months in the Physics Department, Fudan University, Shanghai, where he was involved with the building of an online encyclopedia of all physics. He then joined Photon Design, Oxford, U.K., where he assisted in the design and modeling of a wide range of photonics devices. He is currently with Blaze Photonics, Bath, U.K., where he writes numerical models for the optimal design of various photonic crystal fiber (PCF) applications.

André Vander Vorst (M'64–SM'68–F'86–LF'01) was born in Brussels, Belgium, in 1935. He received the Electrical and Mechanical Engineer degrees and the Ph.D. degree in applied sciences from the Université Catholique de Louvain (UCL), Louvain-la-Neuve, Belgium, in 1958 and 1965, respectively, and the M.Sc. degree in electrical engineering from the Massachusetts Institute of Technology (MIT), Cambridge, in 1965.

From 1958 to 1964, he was involved with fast switching of magnetic cores. From 1964 to 1966, he worked under a NATO Fellowship, first at MIT, then at Stanford University, both in the field of radio-astronomy. In 1966, he founded the Microwave Laboratory, UCL, which he is currently heading, beginning with research on loaded waveguides and cavities. The laboratory currently conducts research on atmospheric transmission and diffraction up to 300 GHz, the methodology of designing and measuring active and passive circuits up to 100 GHz, and microwave bioelectromagnetics, namely, the transmission between the peripheral and central nervous systems, using microwave acupuncture as a stimulus. While with UCL, he has been Head of the Electrical Engineering Department (1970–1972). Dean of Engineering (1972–1975), Vice-President of the Academic Council of the University (1973–1975), and President of the Open School of Economic and Social Politics (1973–1987). He is currently associated with the UCL, where he became an Assistant (1958), Assistant Professor (1962), Associate Professor (1968), and Professor (1972). He has authored or coauthored three textbooks, several chapters, and a variety of scientific and technical papers in international journals and proceedings.

Dr. Vander Vorst is a member of the National Committee of the URSI and of various committees on communications, microwaves, and education. He has been active in IEEE Region 8, as well as in the European Microwave Conferences. He is also a member of Academica Europaea and The Electromagnetics Academy. He was the 1986 recipient of the Sitel Prize and the 1994 IEEE Microwave Theory and Techniques Society (IEEE MTT-S) Meritorious Service Award.